Supplementary Material

Behavior-dependent short-term assembly dynamics in the medial prefrontal cortex

Shigeyoshi Fujisawa, Asohan Amarasingham, Matthew T. Harrison, and György Buzsáki

CONTENTS

§1 Supplementary note

Behavioral training methods.
Adult male (3-5 months old) rats were trained in an odor-based delayed matching-to-sample task prior to surgery. The training apparatus was a modified figure-8 T-maze with a start area where the sample odors (chocolate or cheese) were presented and goal arms, which contained the reward. After consumption of the reward the rats could freely return to the start arm and initiate a new trial (Fig. 1B). The animals were required to nose-poke into a hole in the start box and the odor cue was given. If the cue was cheese odor, a piece of cheese (300mg) was given at the end of the right arm as reward. If the cue was chocolate, the reward was a piece of chocolate (300mg) at the left. Because the reward was placed in the goal arm prior to the trial initiation by the rat, its odor could serve, in principle, as an undesirable spatial cue. To control for this, pieces of both rewards were set in both arms. However, while the correct reward was accessible, the other ("odorant distractor") was covered with a meshed metal bowl to prevent rat from accessing it. In the home-cage, access to food was not restricted, though water was withheld for 12 hours for the purpose of controlling appetite for food. The rats were given water before the session until they were fully satisfied. The reward types in the side arms varied across rats. Rats were trained in 2 stages. For 10 days, they were pre-trained in a small T-maze (with stem length of 30cm). After pre-training, they were retrained in the figure-8 T-maze (Fig. 1B). Rats learned this task with ~85% accuracy within approximately 10 days. Four rats with a performance better than 85% correct choices in 5 consecutive days were chosen for surgery. In the recording sessions, the mean correct performance was 91.9 %.

Histological localization of recording sites
Because of the small volume of the silicon probe shank and its sharp profile, the track of the shanks can be rarely found in histological sections even several weeks after implantation. To facilitate track identification, the back of the shanks was painted with DiI prior to implantation. To identify the depth location of a specific recording site, a small current (2 μA for 3 sec) was passed through the platinum-iridium recording pad of the probe one or two days prior to sacrificing the animals. The rats were deeply anesthetized and perfused through the heart first with 0.9% saline solution followed by 4% paraformaldehyde solution. The brains were sectioned by a Vibroslice at 60 μm in the coronal plane. Sections were mounted on slides, Nissl-stained, and cover-slipped. The tracks of the silicon probe shanks were reconstructed from multiple sections. The combination of these labeling and histological methods allowed for the post-mortem identification of the tracks and recording sites (Fig. 1A; Fig S1).

Number of sampled neurons
On the basis of quantitative neuron counts in different layers of the subdivisions of the mPFC (Table 2 in Gabbott et al. 2005), we estimate that in a cylinder with a radius of approximately 60 μm radius surrounding a single shank approximately 60-100 neurons reside in layer 2/3 and 60 in layers 5. In

contrast, the numbers of neurons recorded physiologically were substantially less. Whereas damage made by the penetration of silicon probes cannot be excluded (Claverol-Tinture & Nadasdy, 2004), it is unlikely that damage alone can account for the low percentage of clusters recorded. First, tracks made by silicon probes are difficult to visualize in Nissl-stained sections even several months after implantation. In fact, DiI staining and lesions through the recording sites were important prerequisites for track identification. Second, after positive identification of the track, the cell density surrounding the track was not visibly different from other areas. Localized loss of >30% of neurons would be quite striking in Nissl-stained section due to both the absence of neuronal cell bodies and the presence of strong basophilic staining of glia (Cavazos et al., 1994). Finally, the 8 recording sites of all 8 shanks could rarely be placed optimally in the cell body rich depth of a given layer, resulting in a large variability of the number of cell clusters from each shank. An alternative explanation for the low number of recorded neurons is the insulating nature of the silicon probe shank. Modeling studies indicate that the carrier substrate of the probe may function as an ohmic insulator, which shields electrical flow from neurons behind the shank to the recording sites, effectively reducing the number of observable neurons by half (Moffit and McIntyre, 2005). According to this model, the number of unit clusters recorded by the best shank in our recordings represents approximately 30 to 50% of all neurons in a 60-μm radius cylinder of mPFC tissue. The remaining neurons are expected to be silent or emitted too few spikes during the experiment to recognize them as separate clusters. The high percentage of physiologically identified putative inhibitory interneurons in the surveyed volume (~37%) further supports the suggestion of silent neurons since mechanical damage should equally affect both pyramidal cells and interneurons. Taking into consideration of the silent/slow firing principal cells, the predicted fraction of interneurons can be estimated as 18%, which agrees well with the 17% GABAergic neurons in quantitative anatomical studies (Gabbott et al., 1997).

Potential caveat with the cross-correlation method

Ren et al., (2007) have shown recently that action potentials generated in a single layer 2/3 pyramidal (excitatory) neuron in the mouse visual cortex can occasionally evoke large, constant-latency inhibitory postsynaptic currents in other nearby pyramidal cells. The authors hypothesized that this effect is mediated by axo-axonic ionotropic glutamate receptor–mediated excitation of the terminals of inhibitory interneurons, which connect to the target pyramidal cells. The implication of this hypothesis is that presynaptic neurons in our inhibitory short-latency cross-correlograms may represent pyramidal cells rather than inhibitory interneurons. While our findings cannot exclude such a possibility, we think it is unlikely that such interactions would be responsible for most effects we observed. First, paired recordings from neocortical pyramidal cells and target interneurons showed high reliability of synaptic transmission (Holmgren et al., 2003; Somogyi et al., 1998; Thomson and Bannister, 2003). Similarly, previous studies in the hippocampus in vivo revealed high spike-transmission probabilities between pyramidal cells and interneurons either by cross-correlation or by intracellular stimulation of the presynaptic pyramidal neuron (Csicsvari et al., 1998; Csicsvari et al., 1999; Marshall et al., 2002). Second, cross-correlation between thalamocortical and putative neocortical interneurons identified monosynaptic excitatory connections (Swadlow & Gusev, 2001). Third, the width and waveshape of the presynaptic spikes in inhibitory interactions were significantly different from those of the presynaptic spikes in excitatory interactions (Barthó et al., 2004), suggesting that they represent two different cell populations.

A different argument against the spike transmission probability method is that it is brought about by a common input (“third party”) and the precise delays in the histograms reflect axon conduction delays. In addition to the above presented reasons, further considerations argue against the third party explanation. First, the delays due to propagation of action potentials are expected to be much shorter for neighboring neurons than the putative monosynaptic delays presented in our paper. Second, axon conduction delays cannot account for our consistent finding that in putatively connected pairs the post-synaptic partner was often a putative interneuron. We have never observed pairs in which a putative interneuron spiked reliably at a fixed latency before a putative principal cell or another putative interneuron. According to the third party explanation, such patterns should be observed at equal probability. Third, we found putative synaptic inhibition (spike suppression) at latencies similar to excitation. The third party excitation model

cannot account for such suppression of spiking.

The 1-2% connection probability we detected between the physiologically identified nearby (<200 μm) pyramidal cell-interneuron pairs by the cross-correlation method is an underestimate for several reasons. First, spikes emitted within 0-1 msec by neurons recorded with the same shank were ignored because of the refractory period of the spike detection method. Second, the cross-correlation method detects only spike transmission or suppression, rather than EPSPs or IPSPs, and likely fails to detect subthreshold excitatory connections and weaker inhibitory connections. Finally, because inhibition with extracellular methods can be inferred only indirectly, it may not be assessed correctly when members of the neuronal pair fire at low rates. These caveats can explain why previous estimations of local connectivity between pyramidal cells and interneurons provided by paired intracellular recordings in vitro have produced values several times higher than ours (Gibson et al., 1999; Holmgren et al., 2003; Thomson 2003; Markram et al., 2004; Thomson and Lamy, 2007).

Putative monosynaptic connections between two pyramidal cells, detected by jitter techniques, were even more rare (detected primarily in layer 5) than reported in vitro. The likely reason is the weaker synapses between pyramidal neurons than between pyramidal cells and interneurons, the higher spike threshold in pyramidal cells, and/or the much larger latency jitter of evoked spikes in pyramidal cells (Pouille & Scanziani, 2004; Thomson & Lamy, 2007). Although single spike-evoked EPSPs in pyramidal cells are typically small and slow rising, occasional connections with >5 mV unitary EPSPs have been observed in layer 5 pyramidal cell pairs in vitro (Buhl et al., 1997; Mason et al., 1991; Reyes et al., 1998; Thomson and Deuchars, 1997; Wang et al., 2006; Hempel et al., 2000; Thomson et al., 2002; Markram et al., 1997; Holmgren et al., 2003; Kapfer et al., 2007). Despite the stronger synaptic connections between pyramidal cells within layer 5, compared to other layers, single neurons rarely discharge their postsynaptic target pyramidal cells in vitro and when they do, the onset latency of the spikes are strongly variable (Hempel et al., 2000; Wang et al., 2006; Thomson & Deuchars, 1997). The low impedance of neurons in the in vivo environment (Pare et al., 1998), however, may be favorable for decreasing the duration of EPSPs and, therefore, the temporal precision of spiking. In addition, the larger fraction of putative pyramidal-pyramidal connections in layer 5 in our study can be explained by the high incidence of reciprocal connections among subsets of pyramidal cells in mPFC (Wang et al., 2006). These considerations explain why the majority of anatomical connections has remained undetected by the spike transmission probability method. Despite these caveats, the present circuit analysis approach demonstrated that relatively large fractions of the recorded neurons were synaptically connected, and allowed us to examine the behavior-dependent modifications of these connections.

§2 Supplementary figures (Fig S1-16)

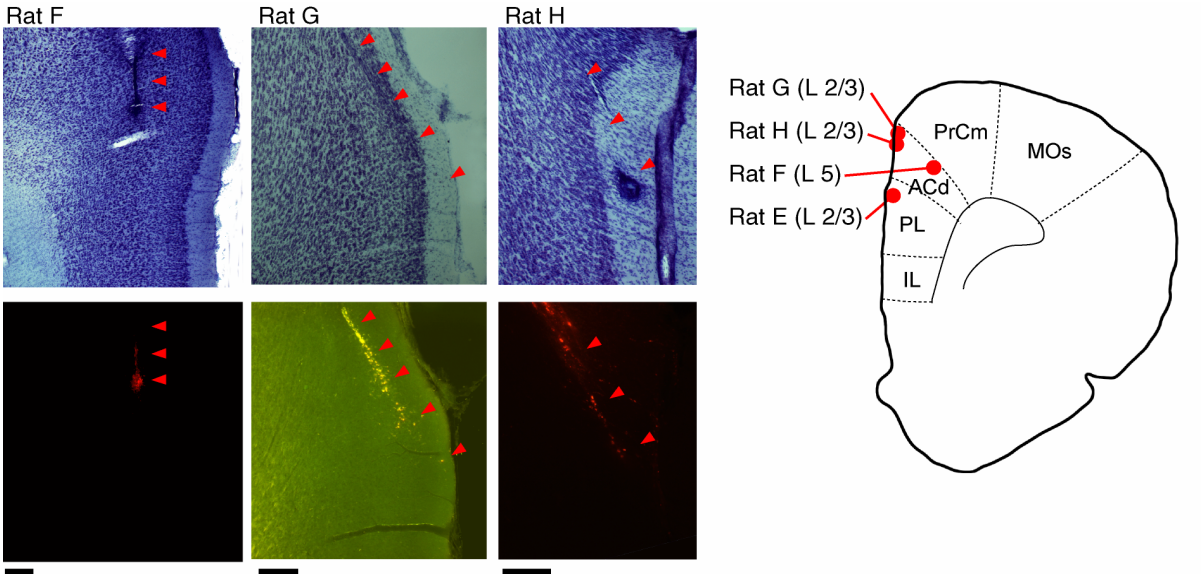

Supplementary Fig 1. Silicon probe recording site positions of each rat. Probe shank locations in rat E are shown in Fig. 1A. Arrowheads, DiI-labeled tracks and corresponding tracks in Nissl-stained sections. DiI was applied on the back side of silicon probe before implantation. Scale bar: 250 μm. Right, summary of recording site subregions and layers in each rat.

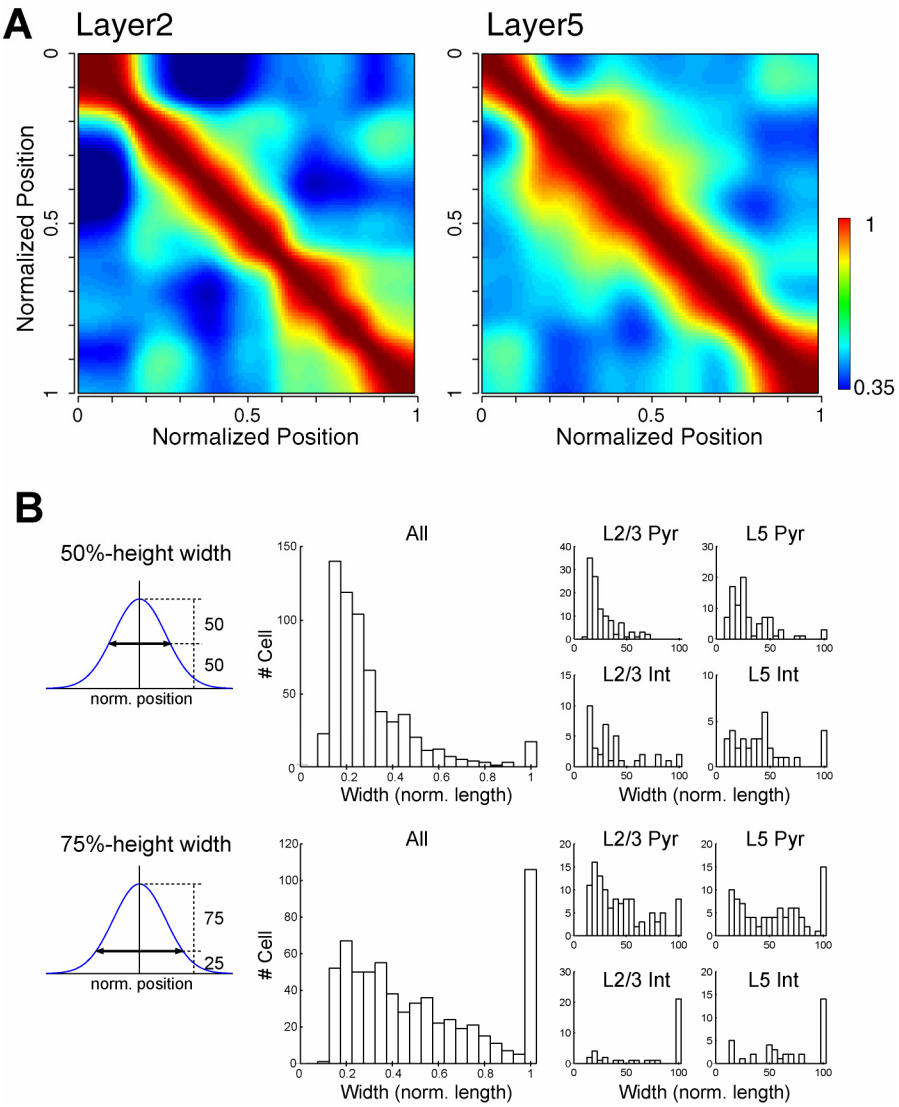

Supplementary Fig 2. Life time (spatial extent) of the firing activity of PFC neurons during the task behavior.
(A) Population vector analysis. Cross-correlation matrices for layer 2/3 and layer 5 neurons. Neuronal populations were relatively evenly correlated throughout the maze segments with 0.18(41cm) ± 0.087(29cm) (L2/3) and 0.27(62cm) ± 0.13(30cm) (L5) in normalized length. (B) The distribution of spatial extent of the firing activity of single neurons in different cell groups. The spatial extent (width) is defined by the 50% (*top*) or 75% (*bottom*) boundaries of the peak height in PSTHs.

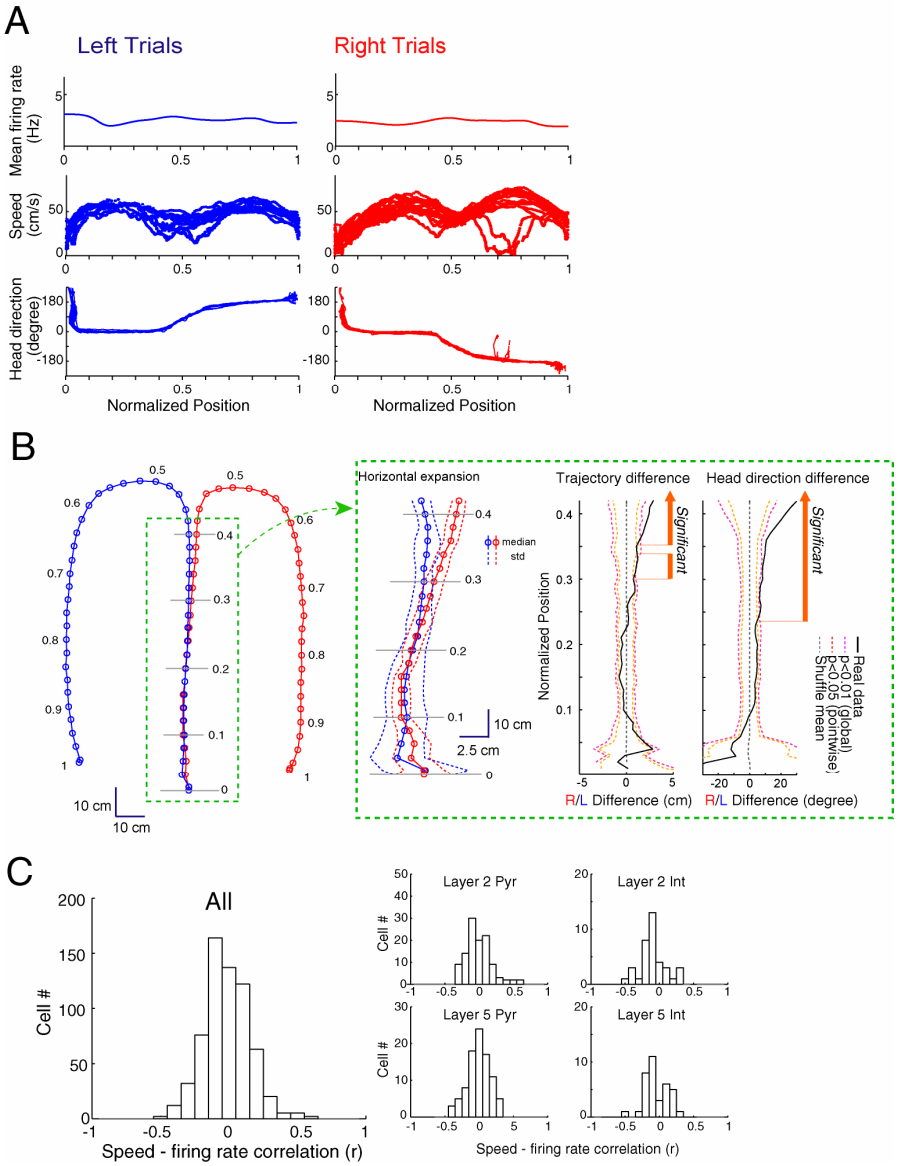

Supplementary Fig 3. Running speed, head position and movement trajectories. (A) Mean firing rate (as in Fig. 2B), speed, and head direction during right and left trials across all neurons during the session analyzed in Figure 2A (layer 2/3). Although speed changed systematically in different maze segments, this change did not correlate with the overall firing rate (which remained steady throughout the trial). (B) Run trajectories during the task behavior. In the stem area of the maze, the trajectories of right and left trials overlapped. Significant separation of left/right trajectories and head directions emerged at position 0.30 and 0.24, respectively ($p<0.01$). Significant differences were computed by the multiple hypothesis testing permutation test (shuffling the labels of left/right trials; see Experimental procedures and Fig S12). Thus, firing pattern differences in maze segments 0 to 0.24 are not explained by differences in head position or orientation. (C) Correlation between firing rates and movement speed. Trials were divided into 0.5 second bins, and the average firing rate and running speed in each bin was tabulated. The correlation coefficient for firing rate and speed was then computed for each neuron. The histograms for all neurons and neuronal subgroups are displayed above. The symmetry of these histograms around 0 suggests that, unlike in the hippocampus, this population of neurons does not exhibit a net positive relationship between firing rate and speed.

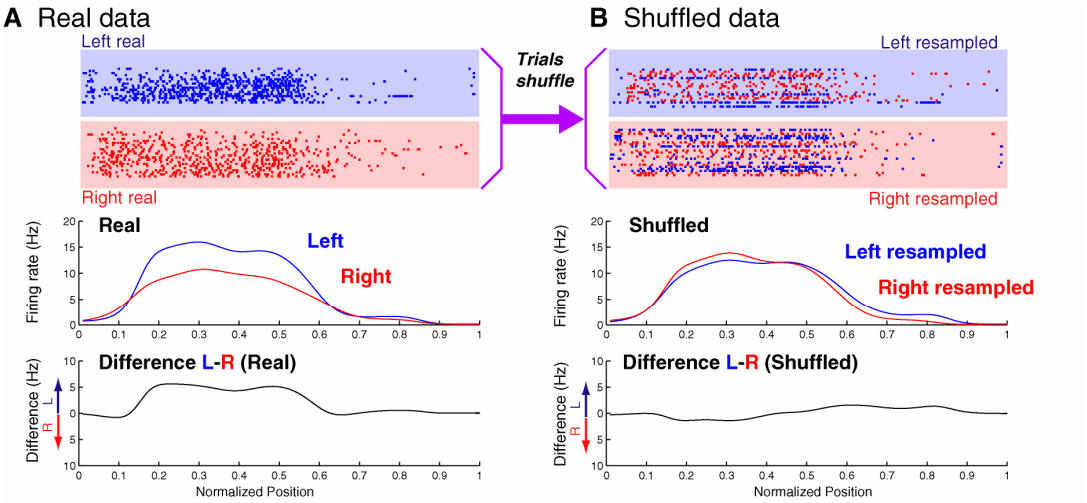
A Real data
Left real
Right real
Trials shuffle
B Shuffled data
Left resampled
Right resampled
Real
Left
Right
Firing rate (Hz)
Difference L-R (Real)
Difference (Hz)
Normalized Position
Shuffled
Left resampled
Right resampled
Difference L-R (Shuffled)

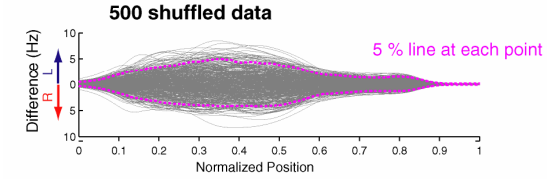
C Pointwise bands
500 shuffled data
5 % line at each point
Difference (Hz)
Normalized Position

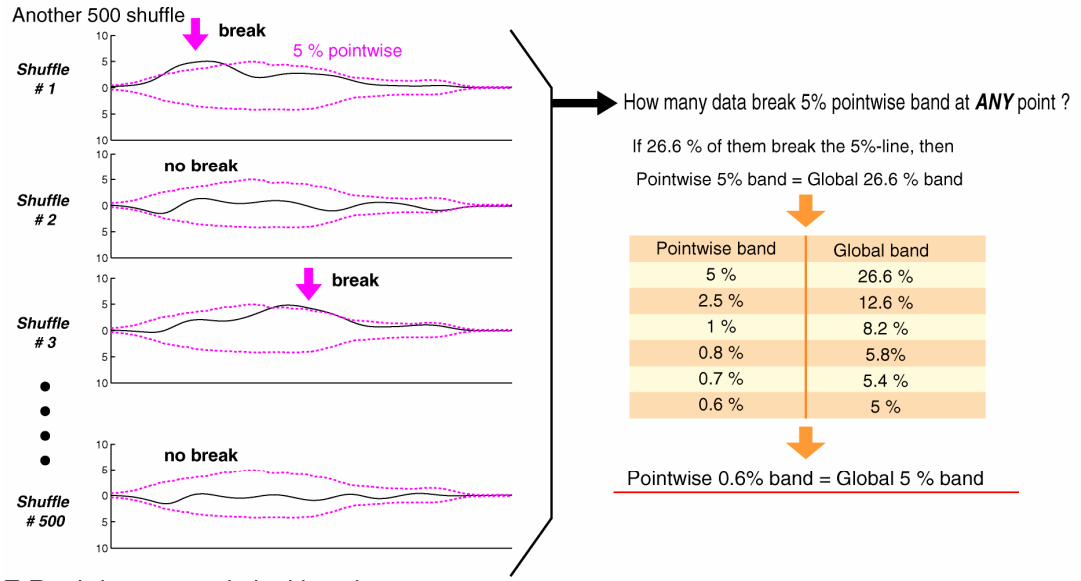
D Global bands
Another 500 shuffle
Shuffle # 1
break
5 % pointwise
Shuffle # 2
no break
Shuffle # 3
break
Shuffle # 500
no break
How many data break 5% pointwise band at ANY point ?
If 26.6 % of them break the 5%-line, then
Pointwise 5% band = Global 26.6 % band
Pointwise band
Global band
5 %
26.6 %
2.5 %
12.6 %
1 %
8.2 %
0.8 %
5.8%
0.7 %
5.4 %
0.6 %
5 %
Pointwise 0.6% band = Global 5 % band

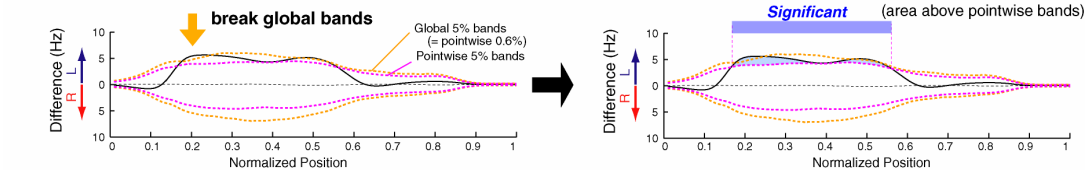
E Real data vs statistical bands
break global bands
Global 5% bands
(= pointwise 0.6%)
Pointwise 5% bands
Difference (Hz)
Normalized Position
Significant
(area above pointwise bands)

Supplementary Fig 4. Identifying distinct firing patterns of neurons under different conditions (Left vs. Right)
(see also, Experimental Procedures in the main text; Amarasingham et al., 2007)

(A) PSTHs in Left & Right trials, and their difference as a function of position.
PSTHs in each condition (i.e. Left or Right trials, $\lambda_L(x)$, $\lambda_R(x)$) are computed as a function of position, by using the equation (E1, in Experimental procedures in the main text). Then we compute the difference $D_0(t) = \lambda_L(x) - \lambda_R(x)$ (E2). Note, in our analyses, the histogram of spike events from multiple trials are plotted as a function of position (mean rate curves) or distance from the start position, not time. Nevertheless, the procedure is analogous to the peri-stimulus time histogram (PSTH). For the shuffling procedure the fundamental idea is same in PSTH (time) and in post-start distance histogram. (If the histograms of the spike events are divided by the occupancy time, the units "1/cm" can be converted to "1/s".) Because PSTH is used more generally, we use this notation.

(B) PSTHs and their difference of shuffled data.
We then randomly permute the Left/Right assignments to $L_1, L_2, \ldots, L_N$, and re-estimate the PSTH's and compute the statistic $D_1(x)$ under the permuted labels. Repeat this process R times to obtain the statistic from the original data, $D_0(x)$, along with the statistic from *resample data*, $D_1(x), \ldots, D_R(x)$.

(C) How to compute pointwise bands.
Using resampled (shuffled) data set, we computed pointwise p-value at each point (equation (E3-5)).

(D) How to compute global bands?
Here the adjusted p-values are computed as following. First, create a family of pointwise acceptance band, one for each possible level of significance. Then, for each pointwise acceptance band see what fraction of the samples lie completely within the band. This fraction is that band's simultaneous acceptance level. The adjusted p-value at an index x can be inferred from the smallest level simultaneous acceptance band that dose not contain the original measurement at index x. In the example of this figure, the global 5% bands correspond to pointwise 0.6% bands. Using the global assessment method, we can establish the lengths of maze segments in our experiments, where spike trains during right and left turns differed significantly. For all neurons, we calculate the shuffled mean, pointwise and global statistics.

(E) Interpretation.
We determined a segment as significant if it satisfied the global criteria of significance but, once established as significant, pointwise criteria were used to determine the segment's (spatial) extent.

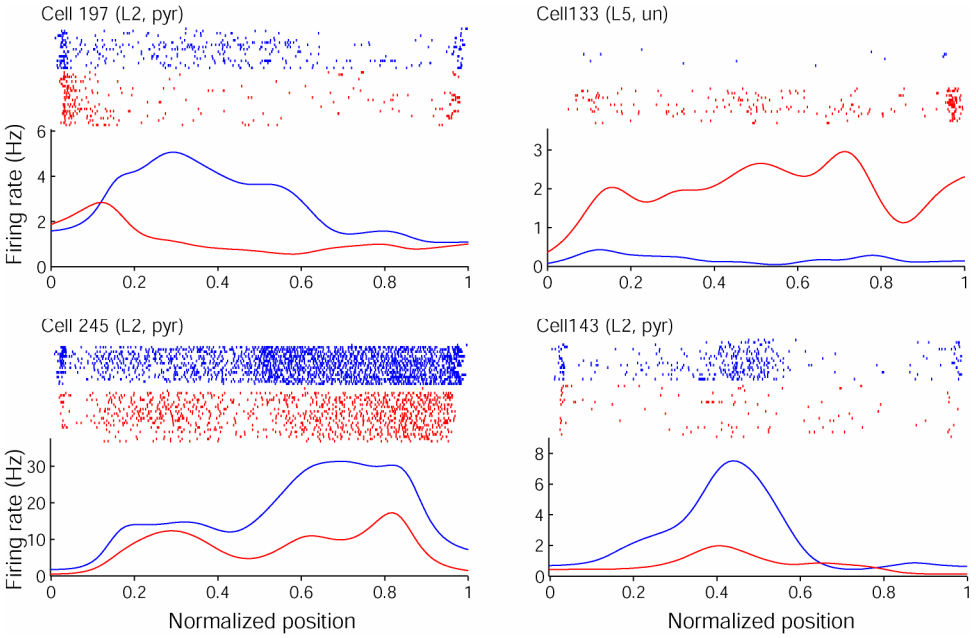

Supplementary Fig 5. Further examples of the firing patterns of PFC neurons. In the delayed odor-place matching task, many neurons showed goal(left/right)-selective firing activity during delay periods and/or other parts of the maze (see also, Figs.1, 2 and 4).

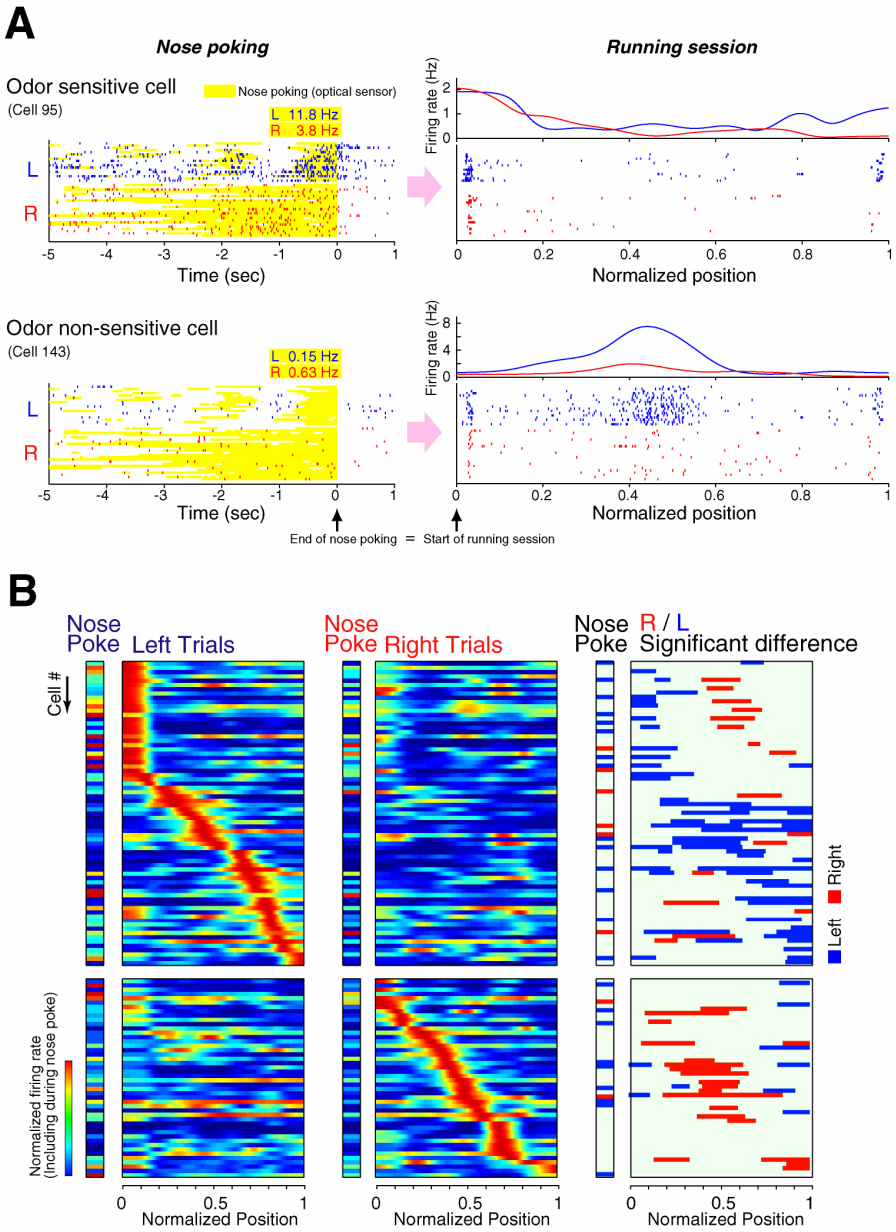

Supplementary Fig 6. Differential odor cue responses of PFC neurons are not related to firing patterns in the maze. (A) Firing patterns of neurons during the nose-poking (*left*) and maze running events (*right*). Yellow shading: duration of nose-poking, detected by a photoelectric sensor. Neuron 95 showed differential odor cue-selectivity but this was not maintained during maze running (*top*). In contrast, neuron 143 was not odor-selective but showed differential (L vs R) firing in the maze (*bottom*). Note that the cue-poking durations are different between left (chocolate odor) and right (cheese odor) trials, perhaps due to the preference of this rat for the cheese odor. (Other rats showed preference for the chocolate odor). The onset of the maze trial is defined as the end of nose-poking, thus maze segment firing rates do not include nose-poking.(B) Group data in a single session (Layer 2/3). Firing patterns of neurons in the maze (same as Fig 2A *left*), compared with nose-poking firing patterns. Although 26% of neurons showed significant odor preference (t-test, $p<.05$), such differential activity was independent of the trial-type differential activity in the stem and side arms of the maze.

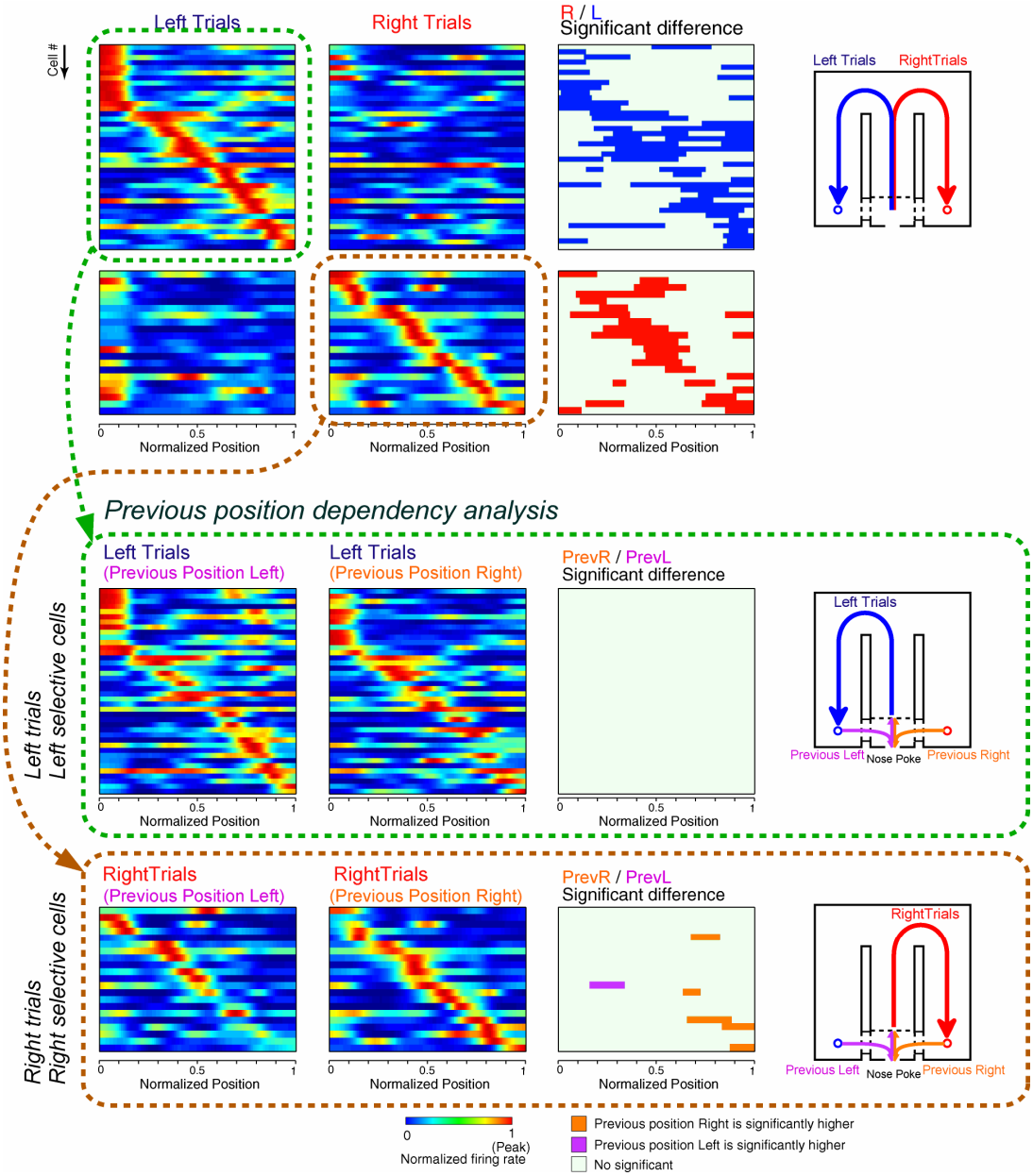

Supplementary Fig 7. Dependence of firing patterns on previous reward location (layer 2/3). The order of odor cue presentation was randomized, so the goal location was independent from the reward location of the *previous* trial. Here we tested whether the neuronal activities were dependent on the previous reward location ("retrospective" sensitivity). The method for identifying L vs R differences was same as in Fig. 2A (see, also Experimental procedures, Fig 1B, and Fig S6), but here the neurons are ordered according to previous reward locations. For testing significance we shuffled the labels of previous locations. ($P<0.05$; the same method that we use for identifying the PSTH differences in left/right trials. See, Experimental procedures and Fig S12). Note that only a small fraction of neurons show retrospective coding.

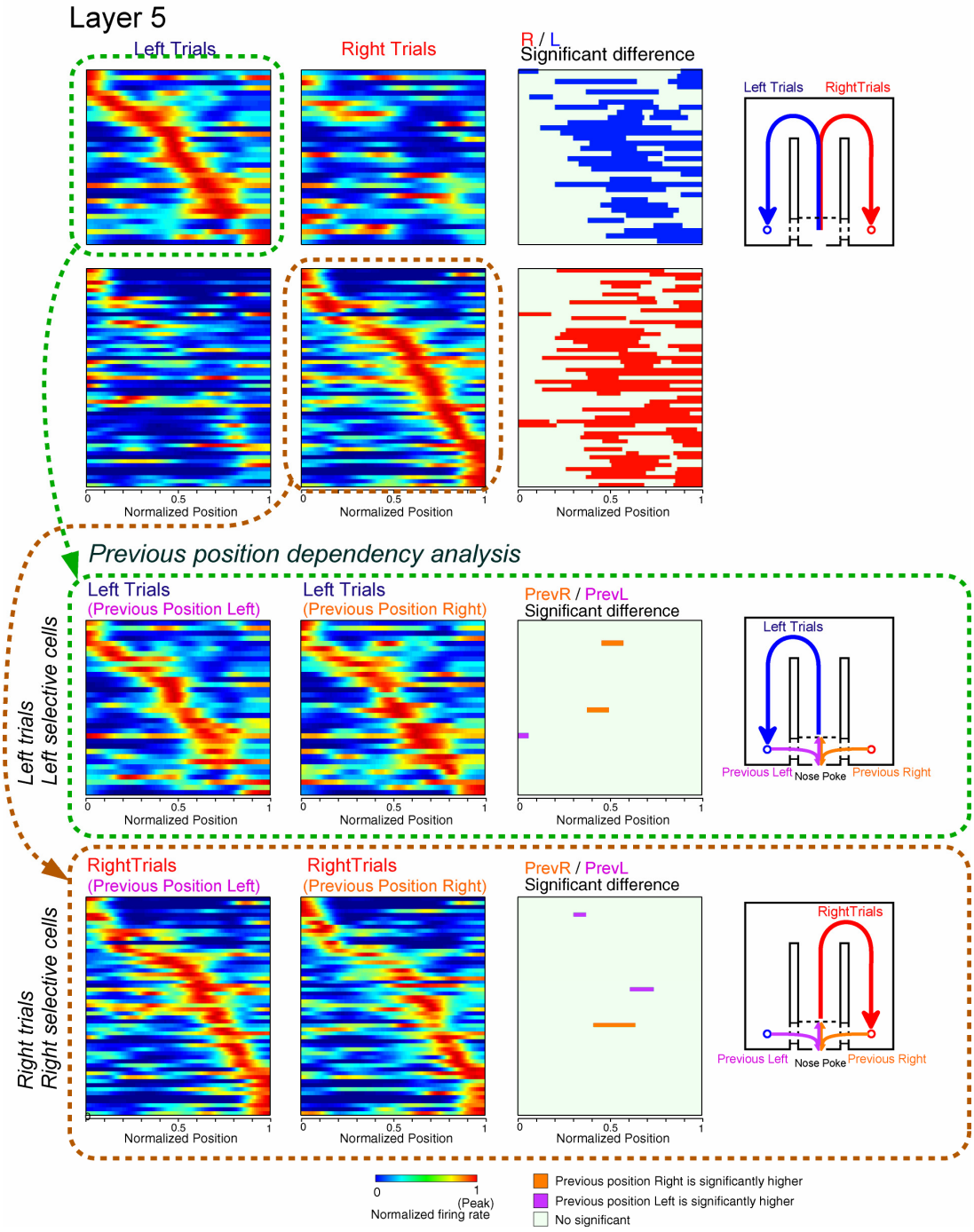

Supplementary Fig 8. Dependence of firing patterns on previous reward location (layer 5). Same analysis as in Fig. S6.

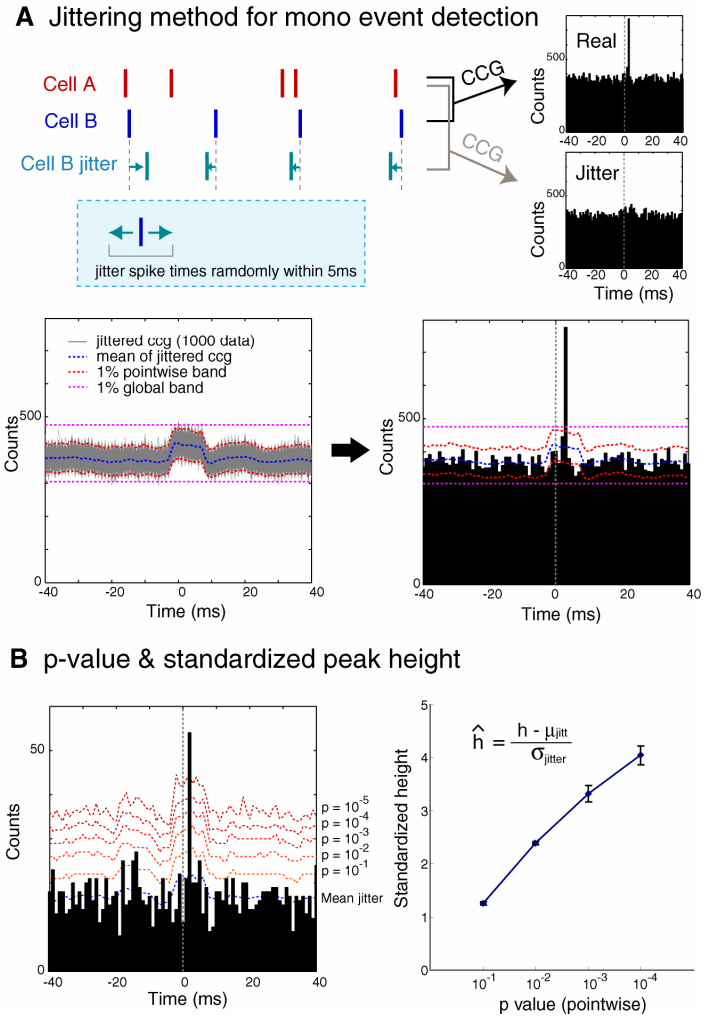

Supplementary Fig 9. Identifying monosynaptic interactions. *Spike jittering method*.
(see also, Experimental Procedures in the main text; Amarasingham et al., 2007)

(**A**) To assess the statistical significance of bin fluctuations in the spike cross-correlograms, spikes of one of the neurons were time jittered by -5 to 5 msec to generate a jittered cross-correlogram (jittered). By repeating the procedure 1000 times, the 99% confidence intervals for each bin (p=0.01) is calculated. In addition, the global (band) significance is indicated and both sets of statistics are superimposed on the original cross-correlogram (lower right). (**B**) Definition of the standardized peak height. Left, Different levels of pointwise significance values computed by the jittering method are shown, superimposed on the original cross-correlogram. Right, Relationship between the height of the significant peak ("synaptic strength", normalized to the mean firing rate) and p values. The standardized peak height $\hat{h}$ is defined as: $\hat{h} = \frac{h - \mu_{jitter}}{\sigma_{jitter}}$

where h is peak height, μ_{jitter} is jittered mean, σ_{jitter} is jittered std. The standardized peak height was proportional to the log p-values computed by jittering method. The standardized peak height is used for quantifying the connection strength, see Fig 6.

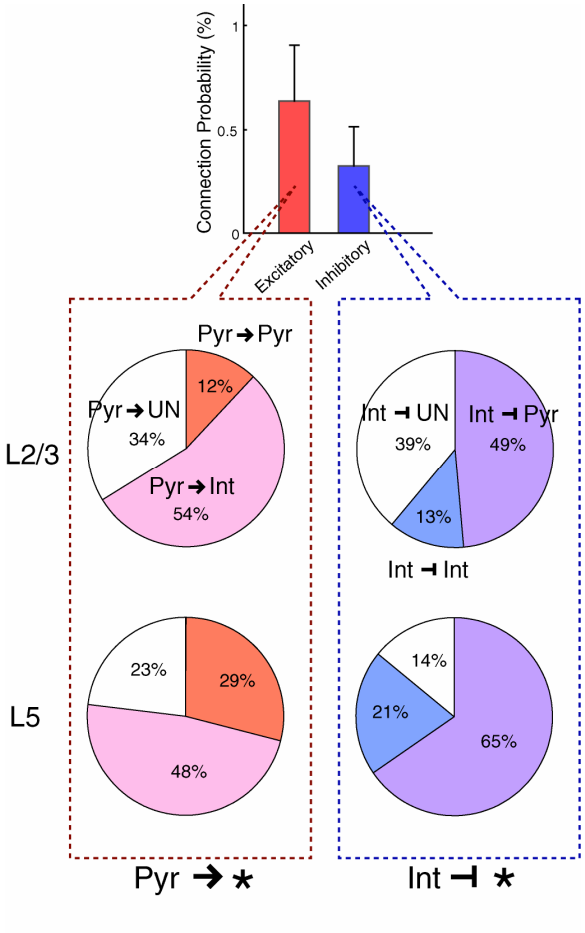

Supplementary Fig 10. Distribution of connection types between putative pyramidal cells (Pyr), interneurons (Int) and unidentified cells (UN). E, excitatory, I, inhibitory synaptic connections.

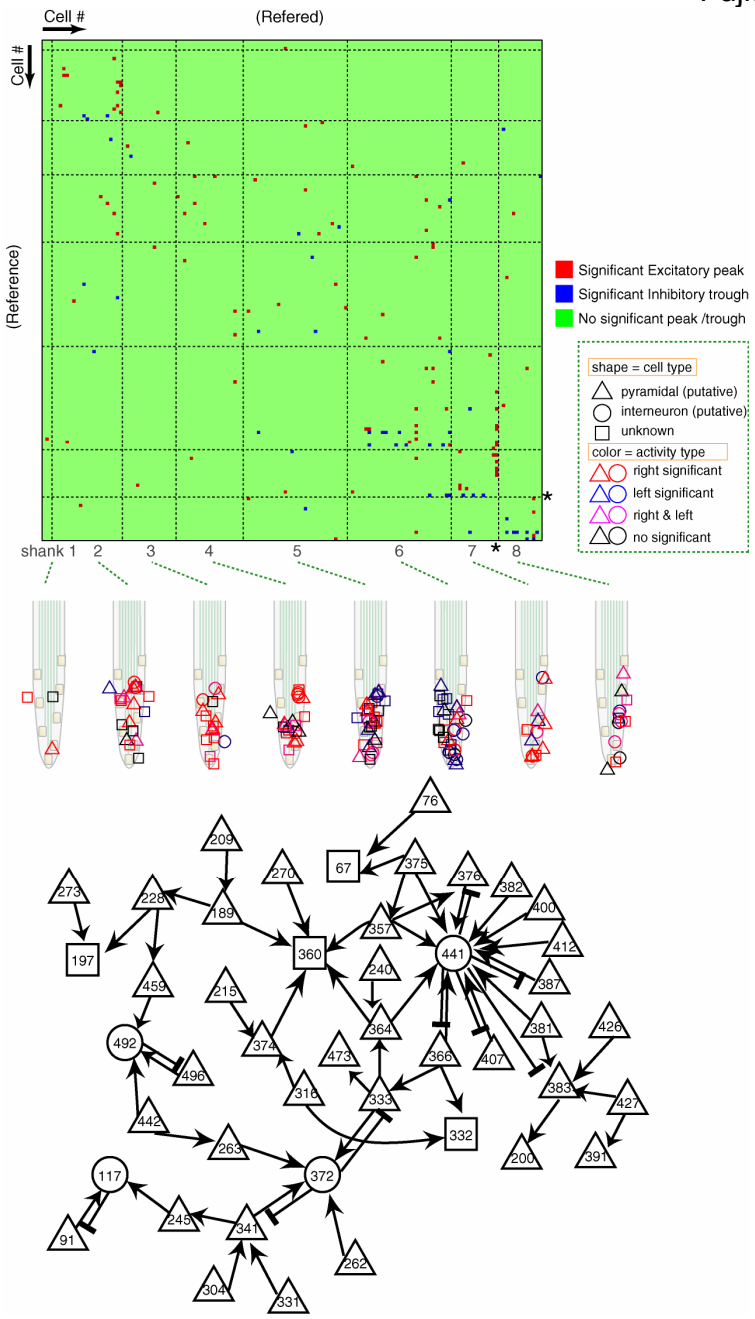

Supplementary Fig 11. Neuronal interactions in layer 5. (B) Cross-correlogram matrix based on simultaneously recorded neuron pairs (n ~ 142^2). Red square, monosynaptic connection (based on significant short-latency peaks) with reference neuron as putative pyramidal cell (n=73), blue square; monosynaptic connection with reference neuron as putative interneuron (n=25); green square, non-significant interaction. **(B)** Calculated two-dimensional position of pyramidal (pyr), interneuron (int) and unidentified (un) neuron types, relative to the recording sites (Barthó et al., 2004). Color-coding indicates whether the neuron discriminated maze segments during right (red), left (blue) or either trajectories in the task. **(C)** Of the physiologically identified neurons a large fraction (45 of 142 total) belonged to a single "hub" of network. Arrows, putative excitatory; stoppers, inhibitory connections. * in A corresponds to interneuron 441 in C, which interacts with several partners.

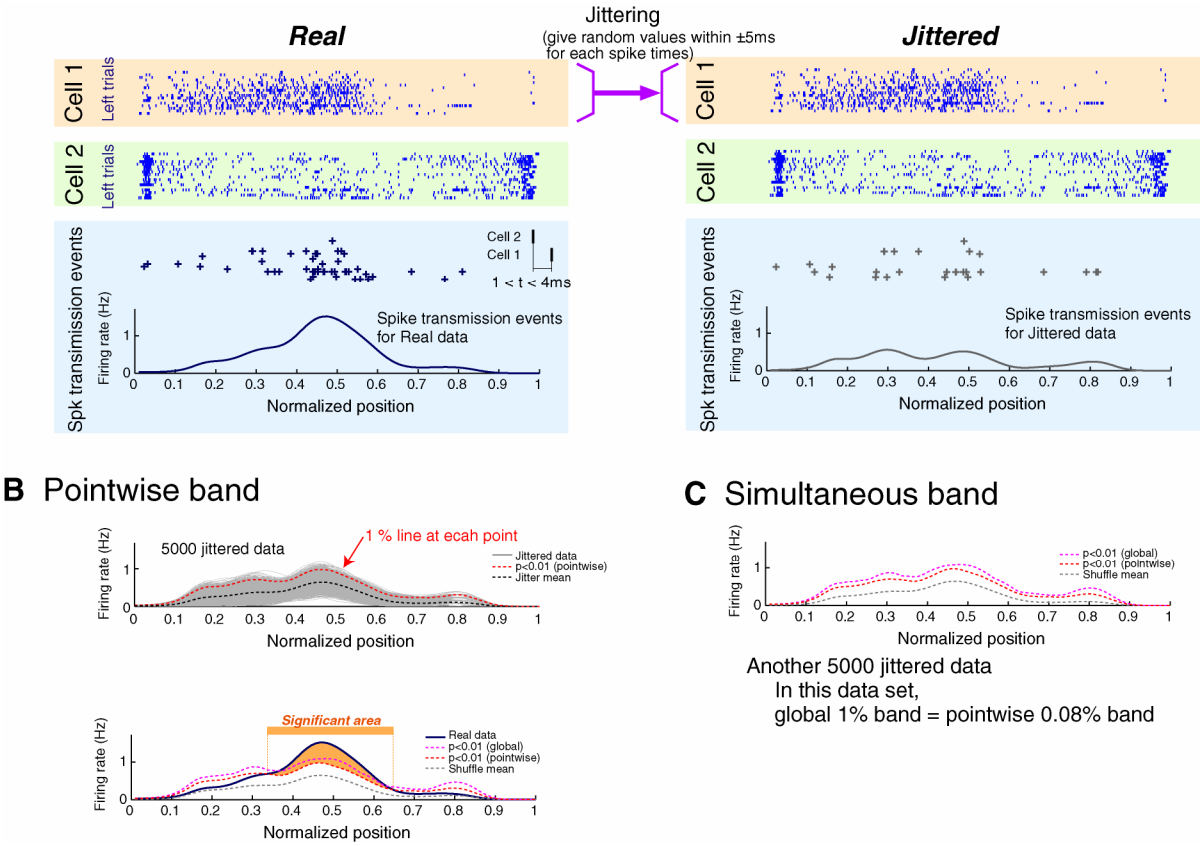

Supplementary Fig 12. Identifying regions of monosynaptic interactions during behavior.
(see also, Experimental Procedures in the main text; Amarasingham et al., 2008)

(A) PSTH of coincident spikes events between cell1 and cell2.
Each spike has a “time” stamp and “position” stamp. Spike transmission events are detected by using time stamps, and plotted by position stamps. The procedure is analogous as presented in Fig. S6 but here we test the significance of spike coincidences of spikes from two neurons and compare them for surrogate (time-jittered) data.
(B) Pointwise assessment of real and jittered data (see Fig S6). Now, by jittering the spike times of cell1, we form a collection of data sets of the PSTH of spike transmission events $\{\lambda_1(x), \lambda_2(x), \ldots, \lambda_N(x)\}$.
(C) Global assessment procedure (as in Fig S6). Data are the same as in Fig. 4.

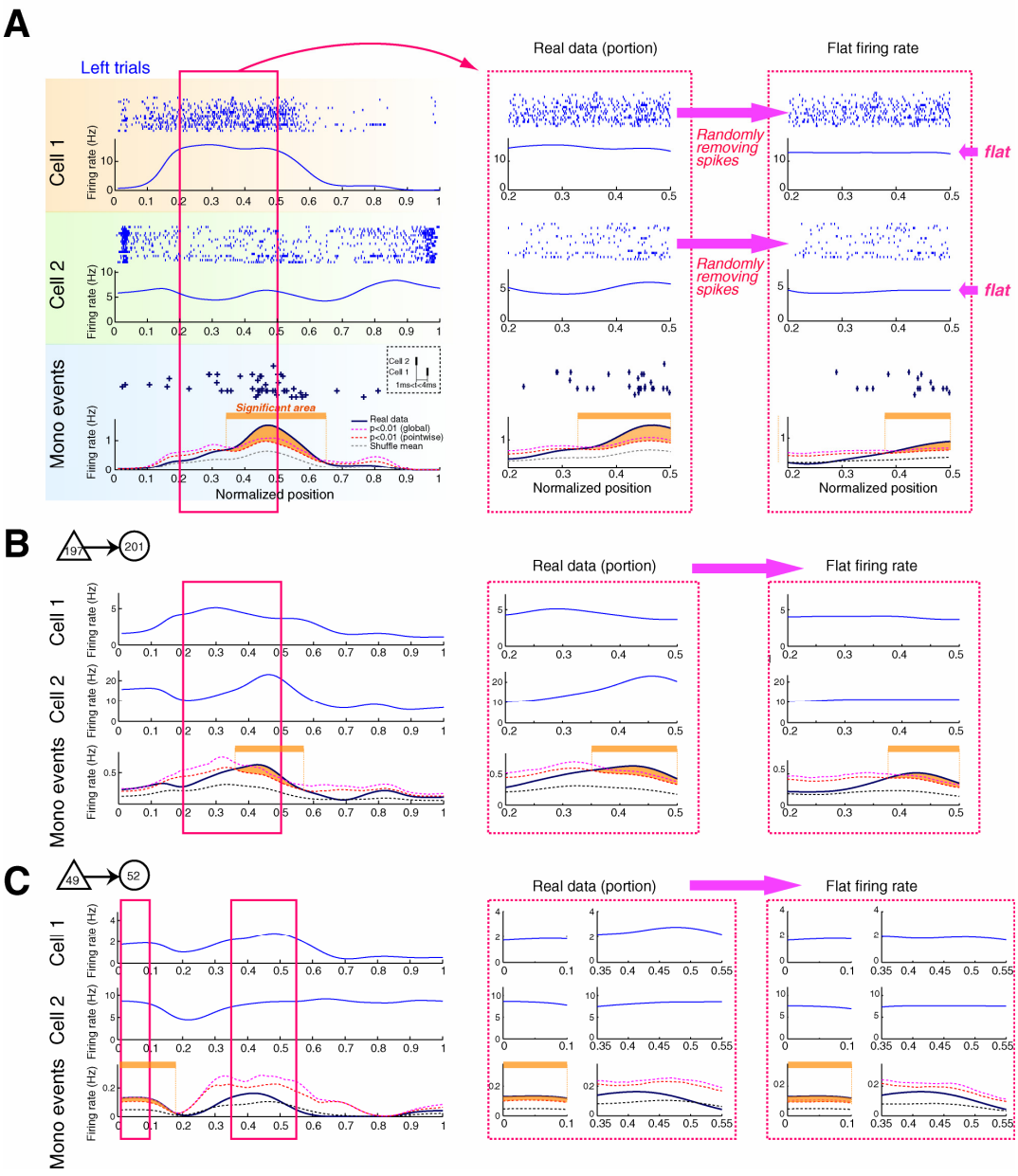

Supplementary Fig 13. Spike rate *"flattening"* method.
(see also, Experimental Procedures in the main text)

We randomly remove spikes from around the peak of the firing rate until the fluctuation of the firing rates becomes less than 10% ($r_{max} - r_{min} < 10$ % of r_{max}). In example (A), we focus on maze segments 0.2~0.5 (box). Spike were removed to produce lower but flat firing rates and the spike transmission probability with the "removed" data set was examined and compared with the original (real) data set. Applying this approach, we indeed find that in several cases the conclusion of position-dependent synaptic efficacy remains unaltered after thinning.

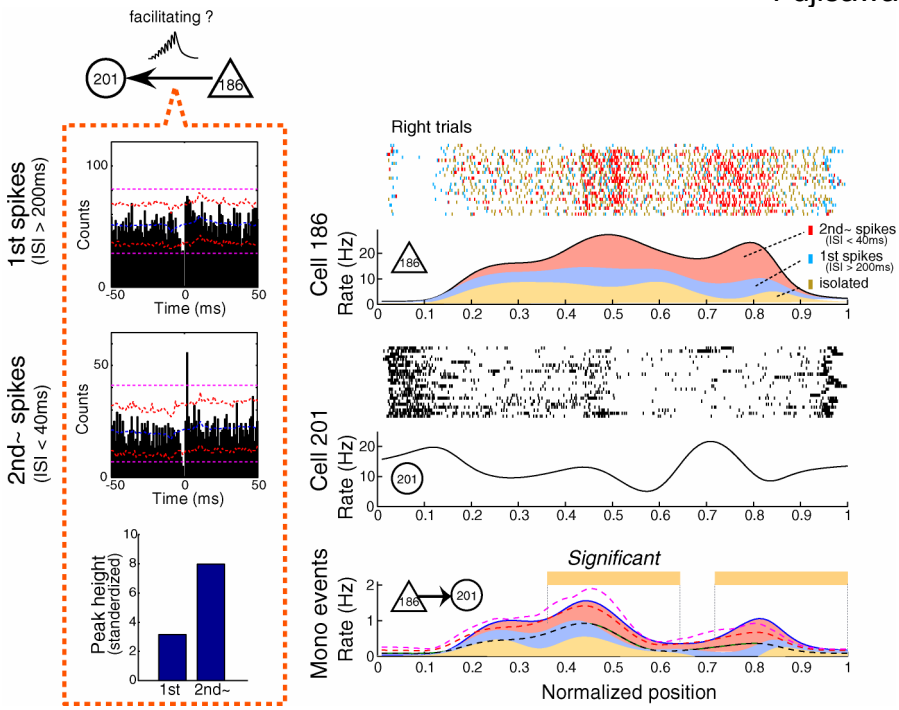

Supplementary Fig 14. Behavior-dependence of spike transmission. (*Left*) Cross-correlograms between neuron pairs (cell 186 and 201) conditioning separately on the 1st and subsequent (2nd~) spikes of trains. “1st spikes”, spikes with long interspike intervals (> 200ms), “2nd~ spikes” spikes with short interspike intervals (< 40 ms). The rate-normalized height of the monosynaptic peak transmission was used to quantify synaptic ‘strength’ (same as in Fig. 6B). (*Right top*) Raster plot and mean firing rate of cell 186 (putative pyramidal cell), conditioned separately on the 1st and subsequent (2nd-) spikes of trains. Blue, “1st spikes”; red, ”2nd~ spikes”; yellow, isolated spikes (preceded and followed by >200 msec lack of discharge). (*Right middle*) Raster plot and mean firing rate of cell 201 (putative interneuron). (*Right bottom*) Monosynaptic interaction between the cells as a function of the position, conditioned separately on the 1st and subsequent (2nd~) spikes of trains and isolated spikes of cell 186 (presynaptic cell). The significant positions of monosynaptic interaction show best overlap with the distribution of “2nd~ spikes”.

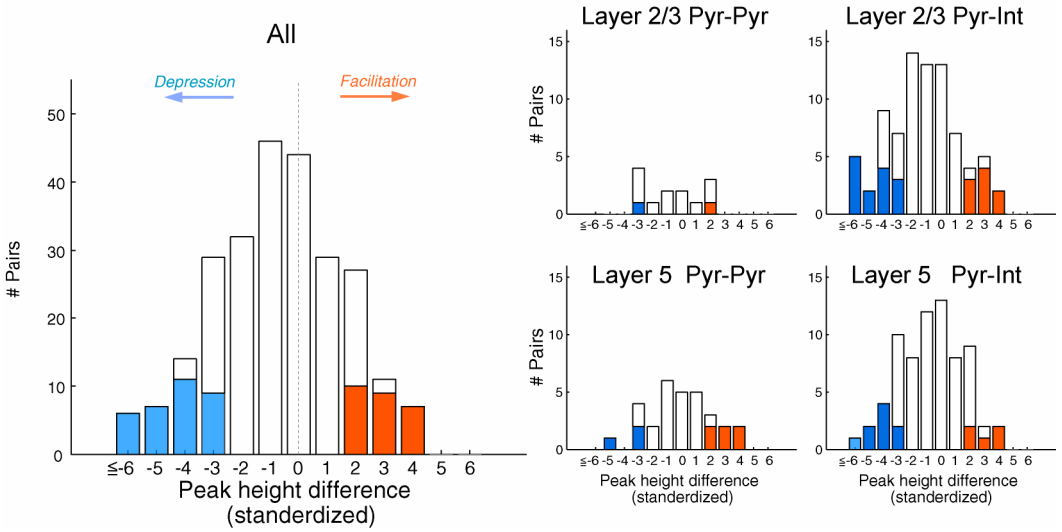

Supplementary Fig 15. Spike transmission efficacy depends on the firing pattern of the presynaptic neuron (See, Fig 6). Distribution of peak height differences between 1st and subsequent spikes in all neuron pairs in different layers (layer 2/3 or 5) and in different connection types (Pyr-Pry or Pyr-Int).

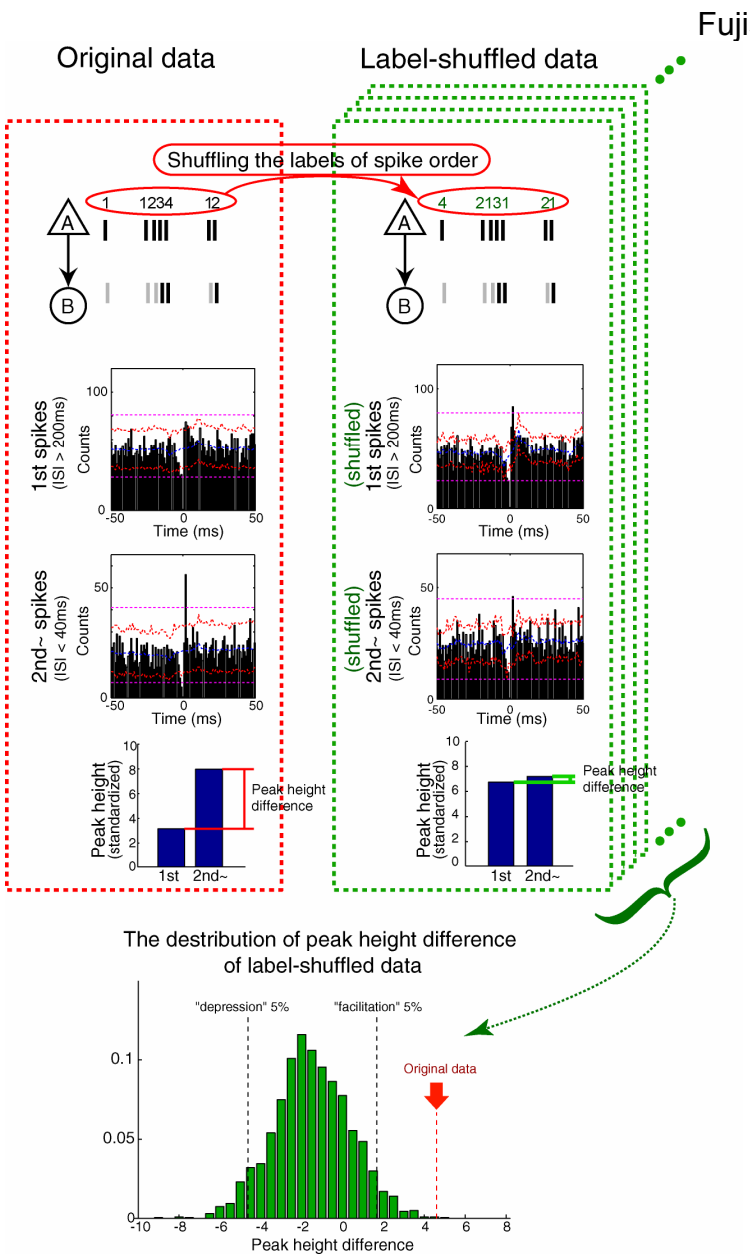

Supplementary Fig 16. Identifying whether spike transmission efficacy depends on the firing pattern (spike order) of the presynaptic neuron.

To assess whether spike transmission efficacy depends on the firing patterns of the presynaptic neuron, a permutation test was used. First we put the label of spike order on each presynaptic spike, based on inter-spike intervals ("1st spikes", spikes with long inter-spike intervals (>200ms), "2nd~ spikes", spikes with short inter-spike intervals (<40ms); see text and Fig. 6). We compute the standardized peak height (see, Fig. S13) for 1st and 2nd~ subsets, and use the peak height difference as a *measure* (*top left*). We then randomly shuffle the 1st, 2nd~ spike labels, and re-estimate the peak height difference under the permuted labels (*top right*). Repeat this process *R* times to obtain the statistic from the original data along with the statistic from resampled data (*bottom*).

References

Amarasingham,A., Harrison,M.T. & Geman,S. Jitter methods for investigating statistical dependencies in neural data, Cosyne, Utah (2007).

Bartho,P., Hirase,H., Monconduit,L., Zugaro,M., Harris,K.D. & Buzsaki,G. Characterization of neocortical principal cells and interneurons by network interactions and extracellular features. *J. Neurophysiol.* **92**, 600-608 (2004).

Buhl,E.H., Tamas,G., Szilagyi,T., Stricker,C., Paulsen,O. & Somogyi,P. Effect, number and location of synapses made by single pyramidal cells onto aspiny interneurones of cat visual cortex. *J. Physiol. (London)* **500**, 689–713 (1997).

Cavazos,J.E., Das,I. & Sutula,T.P. Neuronal loss induced in limbic pathways by kindling: evidence for induction of hippocampal sclerosis by repeated brief seizures. *J. Neurosci.* **14**, 3106-3121 (1994).

Claverol-Tinture,E. & Nadasdy,Z. Intersection of microwire electrodes with proximal CA1 stratum-pyramidale neurons at insertion for multiunit recordings predicted by a 3-D computer model. *IEEE Trans. Biomed. Eng* **51**, 2211-2216 (2004).

Csicsvari,J., Hirase,H., Czurko,A. & Buzsaki,G. Reliability and state dependence of pyramidal cell-interneuron synapses in the hippocampus: an ensemble approach in the behaving rat. *Neuron* **21**, 179-189 (1998).

Csicsvari,J., Hirase,H., Czurko,A., Mamiya,A. & Buzsaki,G. Oscillatory coupling of hippocampal pyramidal cells and interneurons in the behaving rat. *J. Neurosci.* **19**, 274-287 (1999).

Gabbott,P.L., Dickie,B.G., Vaid,R.R., Headlam,A.J. & Bacon,S.J. Local-circuit neurones in the medial prefrontal cortex (areas 25, 32 and 24b) in the rat: morphology and quantitative distribution. *J. Comp Neurol.* **377**, 465-499 (1997).

Gabbott,P.L.A., Warner,T.A., Jays,P.R.L., Salway,P. & Busby,S.J. Prefrontal cortex in the rat: Projections to subcortical autonomic, motor, and limbic centers. *J. Comp. Neurol.* **492**, 145-177 (2005).

Gibson,J.R., Beierlein,M. & Connors,B.W. Two networks of electrically coupled inhibitory neurons in neocortex. *Nature* **402**, 75-79 (1999).

Hempel,C.M., Hartman,K.H., Wang,X.J., Turrigiano,G.G. & Nelson,S.B. Multiple forms of short-term plasticity at excitatory synapses in rat medial prefrontal cortex. *J Neurophysiol.* **83**, 3031-3041 (2000).

Holmgren,C., Harkany,T., Svennenfors,B. & Zilberter,Y. Pyramidal cell communication within local networks in layer 2/3 of rat neocortex. *J. Physiol. (London)* **551**, 139-153 (2003).

Kapfer,C., Glickfield,L.L., Atallah,B.V. & Scanziani,M. Supralinear increase of recurrent inhibition during sparse activity in the somatosensory cortex. *Nat. Neurosci.* **10**, 743-753 (2007).

Markram,H., Lübke,J., Frotscher,M. & Sakmann,B. Regulation of Synaptic Efficacy by Coincidence of Postsynaptic APs and EPSPs. *Science* **275**, 213-215 (1997).

Markram,H., Toledo-Rodriguez,M., Wang,Y., Gupta,A., Silberberg,G. & Wu,C.Z. Interneurons of the neocortical inhibitory system. *Nat. Rev.Neurosci.* **5**, 793-807 (2004).

Marshall,L., Henze,D.A., Hirase,H., Leinekugel,X., Dragoi,G. & Buzsaki,G. Hippocampal pyramidal cell-interneuron spike transmission is frequency dependent and responsible for place modulation of interneuron discharge. *J. Neurosci.* **22**, RC197 (2002).

Mason,A., Nicoll,A. & Stratford,K Synaptic transmission between individual pyramidal neurons of the rat visual cortex in vitro. *J. Neurosci.* **11**, 72–84 (1991).

Moffitt,M. & McIntyre,C. Model-based analysis of cortical recording with silicon microelectrodes. *Clinical Neurophysiol.* **116**, 2240-2250 (2005).

Pare,D., Shink,E., Gaudreau,H., Destexhe,A. & Lang,E.J. Impact of spontaneous synaptic activity on the resting properties of cat neocortical pyramidal neurons in vivo. *J. Neurophysiol.* **79**, 1450-1460 (1998).

Pouille,F. & Scanziani,M. Routing of spike series by dynamic circuits in the hippocampus. *Nature* **429**, 717-723 (2004).

Ren,M., Yoshimura,Y., Takada,N., Horibe,S. & Komatsu,Y. Specialized inhibitory synaptic actions between nearby neocortical pyramidal neurons. *Science* **316**, 758-761 (2007).

Reyes,A., Lujan,R., Rozov,A., Burnashev,N., Somogyi,P. & Sakmann,B. Target-cell-specific facilitation and depression in neocortical circuits. *Nat. Neurosci.* **1**, 279-285 (1998).

Somogyi,P., Tamás,G., Lujan,R. & Buhl,E.H. Salient features of synaptic organisation in the cerebral cortex. *Brain Res Brain Res Rev.* **26**, 113-35 (1998).

Swadlow,H.A. & Gusev,A.G. The impact of 'bursting' thalamic impulses at a neocortical synapse. *Nat. Neurosci.* **4**, 402-408 (2001).

Thomson,A.M. Presynaptic frequency- and pattern-dependent filtering. *J. Comput. Neurosci.* **15**, 159-202 (2003).

Thomson,A.M. & Bannister,A.P. Interlaminar Connections in the Neocortex. *Cereb. Cortex* **13**, 5-14 (2003).

Thomson,A.M., West,D.C., Wang,Y. & Bannister,A.P. Synaptic connections and small circuits involving excitatory and inhibitory neurons in layers 2–5 of adult rat and cat neocortex: triple intracellular recordings and biocytin labeling in vitro. *Cereb. Cortex* **12**, 936–953 (2002).

Thomson,A.M. & Deuchars,J. Synaptic interactions in neocortical local circuits: dual intracellular recordings in vitro. *Cereb. Cortex* **7**, 510-522 (1997).

Thomson,A.M. & Lamy,C. Functional maps of neocortical local circuitry. *Frontiers Neurosci.* **1**, 19-42 (2007).

Wang,Y., Markram,H., Goodman,P.H., Berger,T.K., Ma,J. & Goldman-Rakic,P.S. Heterogeneity in the pyramidal network of the medial prefrontal cortex. *Nat. Neurosci.* **9**, 534-42 (2006).